Article | Open Access

Energy Materials

Cheng *et al. Energy Mater.* **2026**, *6*, 600084 **DOI:**10.20517/energymater.2026.103

Manipulating surface buffer of transition metal sulfide for robust seawater electrolysis

Shijia Cheng[1,2], Siyuan Tang[1,*], Xiang Ding[1], Nan Jiang[3,*], Haotian Qin[1], Yin Yin[1,*], Fuzhan Song[1,*]

Keywords:
Cost-effective electrocatalyst, transition-metal sulfides, nitrogen-doped carbon layer, seawater splitting, synergistic effect

Citation: Cheng, S.; Tang, S.; Ding, X.; Jiang, N.; Qin, H.; Yin, Y.; Song, F. Manipulating surface buffer of transition metal sulfide for robust seawater electrolysis. *Energy Mater.* **2026**, *6*, 600084. https://dx.doi.org/10.20517/energymater.2026.103

Received: 30 Apr 2026 **First Decision:** 29 May 2026 **Revised:** 21 Jun 2026 **Accepted:** 14 Jul 2026 **Published:** 27 Jul 2026

Academic Editor: Yuping Wu
Copy Editor: Ping Zhang
Production Editor: Ping Zhang

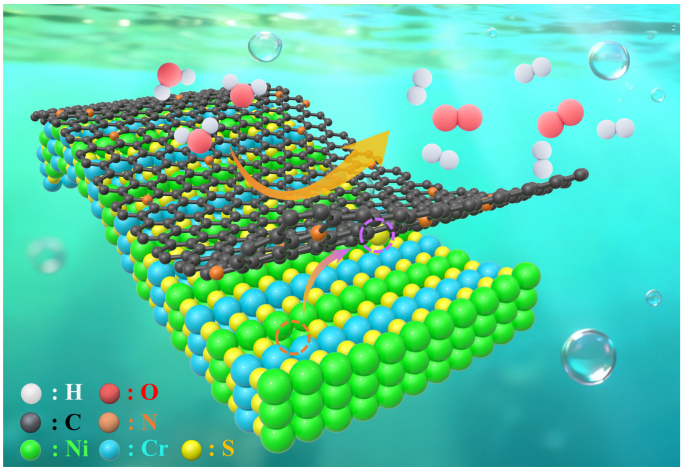

Abstract

Developing highly active and robust transition-metal electrocatalysts for seawater electrolysis is pivotal for industrially relevant green hydrogen production, yet remains a great challenge. Herein, we reported a novel hybrid nickel-chromium sulfide-based electrocatalyst (NiCrS/CN), integrating NiCrS with nitrogen-doped carbon shell encapsulation, to manipulate sulfur migration. Benefiting from nitrogen-doped carbon (C-N) layer interfacial regulation, the obtained NiCrS/CN electrocatalytic system demonstrates an outstanding seawater splitting performance. Accelerating hydrogen evolution reaction (HER) kinetics with corresponding overpotentials as low as 143, 164, and 191 mV to -50, -100, and -200 mA cm^{-2} in alkaline seawater electrolyte, respectively, is observed for the NiCrS/CN electrode. Notably, our NiCrS/CN electrolyzer can stably produce an industrial current density of 50 mA/cm^2 at a potential of 1.40 V, 120 mV lower in energy potential than that of the NiCrS (1.52 V) electrolyzer in an alkaline seawater system. Remarkably, our NiCrS/CN system can stably maintain a superior 1200-hour electrolysis in alkaline electrolyte. Even under seawater conditions, the rationally designed NiCrS/CN electrolyzer can be stably operated for at least 100 h to achieve industrially relevant hydrogen production from seawater splitting. Such a striking performance is

[1]School of Materials Science and Engineering, Jiangsu University, Zhenjiang 212013, Jiangsu, China.
[2]Nanyang Technological University, 50 Nanyang Avenue, Singapore 639798, Singapore.
[3]Department of Chemistry and Chemical Engineering, Guizhou University, Guiyang 550025, Guizhou, China.

***Correspondence to:** Dr. Siyuan Tang, Prof. Fuzhan Song, Prof. Yin Yin, School of Materials Science and Engineering, Jiangsu University, Zhenjiang 212013, Jiangsu, China. E-mail: 2112305054@stmail.ujs.edu.cn; fzsong@ujs.edu.cn; yyin@ujs.edu.cn; Prof. Nan Jiang, Department of Chemistry and Chemical Engineering, Guizhou University, Guiyang 550025, Guizhou, China. E-mail: njiang@gzu.edu.cn

attributed to C-N layer encapsulation, which not only induces a strong synergistic effect to optimize local electronic configuration, but also manipulates an alkaline micro-environment for Cl^- buffer as well as S migration, resulting in a robust industrial-relevant seawater splitting for hydrogen generation.

INTRODUCTION

The global energy transition, as well as environmental challenges, will advance electrocatalytic energy conversion technologies for sustainable renewable clean energy utilization[1-4]. Hydrogen energy, characterized by its high mass energy density along with environmental friendliness, has been deemed a compelling alternative to traditional fossil fuels[5-8]. Among various hydrogen production technologies[9-11], direct seawater electrocatalysis coupled with renewable energy (e.g., solar and wind) offers a convenient strategy to produce industrial-grade green hydrogen gas owing to the vast availability of seawater and zero-emission nature[12-14]. However, in acidic electrolytes, the high concentration of chloride species, as well as the complex composition, will inevitably result in chlorine corrosion together with calcium/magnesium salt precipitation[15,16]. In addition, the undesirable chloride evolution reaction generates corrosive chlorine species with oxidatizing abilities that block the active sites of the catalyst surface. Such a harsh environment will result in electrode deactivation associated with low efficiency of hydrogen production[17]. Conversely, some progress has been recently made on alkaline seawater electrolysis[18,19]. According to the Pourbaix plot, the anodic oxygen evolution reaction (OER) can compete significantly with the chloride evolution reaction (CER) under alkaline conditions, with a theoretical overpotential input of 0.48 V[20,21]. To date, although alkaline seawater electrolysis exhibits significant enhancement in suppressing CER selectivity as well as salt precipitation, it still suffers from sluggish kinetics over two orders of magnitude relative to that in acidic electrolyte, leading to a low energy conversion efficiency[22,23]. As a result, developing low-cost and efficient seawater electrocatalysts with high performance and robust stability is urgent, which could not only reduce the energy barrier of seawater splitting, but also avoid the competitive CER in alkaline solution, achieving industrial-scale hydrogen production for a "hydrogen energy society".

Transition-metal sulfides (TMSs) are widely regarded as promising candidates for seawater electrolysis due to their tunable 3d electronic configuration as well as excellent electrical conductivity[24-27]. Especially, binary transition-metal sulfides-based electrocatalysts have attracted intensive attention due to their localized structural polarization and optimizing the charge redistribution associated with orbital rehybridization[28,29]. In addition, the unique configuration could enable pronounced p-d orbital hybridization coupled with 3d orbitals of transition metal sites and the 3p orbitals of sulfur species, which efficiently facilitates interfacial electron delocalization and accelerates charge transfer for a higher oxidation state of metallic sites. Despite some binary transition metal sulfides-based catalysts demonstrating enhanced electrocatalytic performance, further improvements are still required to match with harsh conditions of a seawater electrolyzer due to structural instability as well as suboptimal thermal-neutral behavior of intermediate species. In detail, TMS-based electrocatalysts undergo surface reconstruction during seawater electrocatalysis, resulting in inevitable sulfur leaching[30]. Long-term sulfur leaching will destroy the structural configuration of sulfur species, leading to the loss of abundant sulfur components and rapid active degradation. In addition, the released sulfur species could block the metallic sites and break the adsorption/desorption balance of intermediate species over the catalytic surface. Recent advances have shown that local micro-environment modulation of the catalyst surface could enable a robust seawater electrolysis[31,32]. Very recently, the introduction of a nitrogen-doped carbon (C-N) shell, as a Lewis base layer, has been explored to manipulate an alkaline local micro-environment of TMS-based electrocatalysts[33,34]. The chlorine coordinated dynamics of the catalyst surface could be effectively suppressed by preferential enrichment of N species to "resist" Cl^- corrosion. Additionally, the C-N overlayers benefit from anchoring leached sulfur atoms via strong C-S bonds at the core-shell heterogeneous region, inhibiting sulfide species dissolution into seawater and enabling robust

seawater electrocatalysis. More interestingly, the incorporation of C-N overlayers could induce a strong synergistic effect to adjust the *d* band center of metallic active sites while optimizing the electrochemical adsorption-desorption intrinsic capability. Such a novel local electronic configuration is prone to hydrogen atom spillover, reducing the energy barrier for H_2O dissociation between TMS actives and C-N layers. Despite these advances, the construction of robust TMS/C-N interfacial electrocatalysts toward electrocatalyzing seawater splitting remains in its early stages.

In this work, we present a novel strategy for manipulating interfacial sulfur migration through constructing a NiCrS/CN heterogeneous electrocatalyst featuring C-N shell encapsulation. The obtained NiCrS/CN electrocatalytic system only requires an ultralow overpotential input of 143, 164 and 191 mV to generate an industrial-grade current density of -50, -100, and -200 mA cm^{-2}, which is 12.20, 15.87 and 19.8 times relative to those of NiCrS (-4.1, -6.3 and -10.1 mA/cm^2), respectively, at the same overpotential input. Furthermore, the assembled NiCrS/CN two-electrode electrolyzer demonstrates a robust industrially relevant operational performance and could be operated for at least 1,200 h and 100 h in alkaline freshwater and seawater electrolytes, respectively. Such a high active and robust electrocatalytic performance is attributed to C-N layers, which not only enhance intrinsic activity by promoting electron delocalization via a strong synergistic effect, but also serve as a Lewis base layer to effectively suppress Cl-induced corrosion and S leaching. This work provides a promising strategy for designing efficient and corrosion-resistant seawater electrocatalysts

EXPERIMENTAL

Synthesis of NiCr

NiCr electrode was prepared by cathodic electrodeposition of NiCr particles on nickel foam (NF). The electrodeposition was performed in a standard two-electrode glassy configuration containing a mixed solution of 2.0 M NH_4Cl and 0.1 M $NiCl_2$ + $CrCl_3$. A piece of NF (0.5 cm × 0.5 cm) was used as the working electrode, and a carbon rod as the corresponding counter electrode. The NiCr deposit was obtained by electrodeposition for 500 s at a constant current density of -1.0 A/cm^2 under N_2 protection. After deposition, the electrode was thoroughly rinsed with deionized water and then vacuum-dried for 6 h, yielding the NiCr electrode.

Synthesis of NiCrS and NiCrS/CN

The NiCrS/CN electrodes were prepared by controlled sulfuration. Thiourea (0.263/0.625 g) was positioned upstream, and NiCr was placed centrally in a tube furnace, ensuring optimal spacing between the reactants. After being flushed with N_2 gas for 2 h, the center temperature of the furnace was rapidly raised to the desired temperature (350 °C, 10 °C/min) and held steady for a precise duration (2 h). Finally, NiCrS/CN were obtained after cooling down to room temperature. NiCrS electrode was synthesized using a similar procedure, with sulfur (0.263 g) rather than thiourea.

RESULTS AND DISCUSSION

The synthetic procedure of NiCrS/CN catalysts was schematically depicted in Figure 1. In brief, a porous NiCr microsphere was cathodically electrodeposited, followed by a thermal treatment process using thiourea (CH_4N_2S) to synthesize NiCrS/CN.

The Raman spectra of NiCrS and NiCrS/CN in Figure 2A confirm different characteristic peaks at 1,405.4 and 1,575.6 cm^{-1}, indicating the formation of C-N overlayers. As depicted in Figure 2B, the diffraction peaks at 31.59°, 38.78°, and 45.31°in spectrum can be well matched with the (200) (211) and (220) crystal planes of NiS_2 (JCPDS No. 11-0099), while the peaks at 34.19° 44.46°and 53.41° can be attributed to the (112) (114) and (300) crystal planes of Cr_2S_3 (JCPDS No. 11-0007). Notably, no carbon diffraction peaks were observed in the

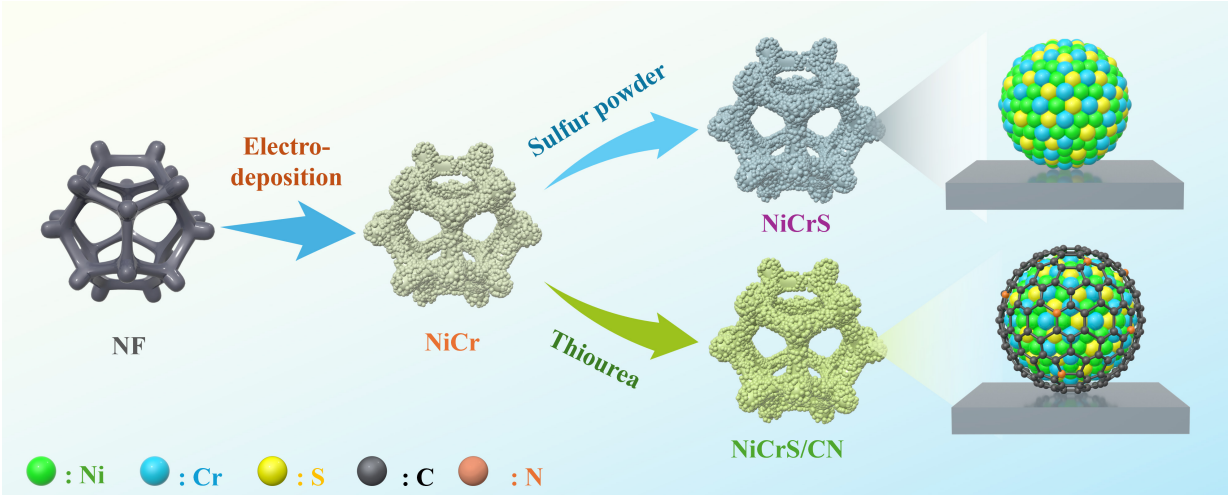

Figure 1. Schematic illustration of the synthesis process of NiCrS/CN. NF: Nickel foam; NiCrS/CN: nickel-chromium sulfide with nitrogen-doped carbon shell.

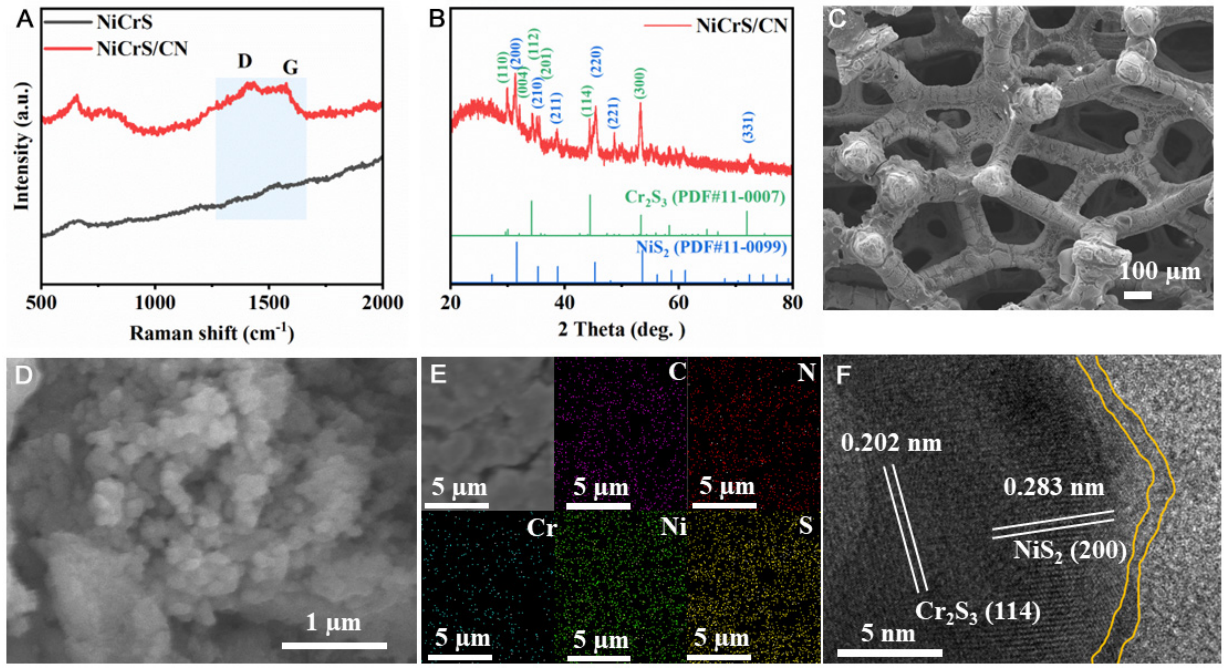

Figure 2. (A) Raman spectra of NiCrS and NiCrS/CN; (B) XRD result, (C and D) SEM images, (E) Element mapping images and (F) HRTEM result of NiCrS/CN. SEM: Scanning electron microscope; HRTEM: high-resolution transmission electron microscopy; XRD: X-ray diffraction; NiCrS/CN: nickel-chromium sulfide with nitrogen-doped carbon shell.

X-ray diffraction (XRD) patterns, indicating that the obtained C-N layer possesses a non-crystalline structure and ultrathin thickness. Scanning electron microscope (SEM) images demonstrate that NiCrS/CN possesses a 3D cotton-like architecture with abundant microspheres stacked [Figure 2C-E]. Such a novel structural feature significantly improves mass transfer ability and facilitates bubble detachment under high current densities, thereby enhancing the overall electrocatalytic performance. High-resolution transmission electron microscopy (HRTEM) results in Figure 2F reveal an ultrathin C-N overlayer (~1.5 nm) encapsulated on the NiCrS surface. The observed interplanar spacings of 0.283 and 0.202 nm are ascribed to NiS_2 (200) and Cr_2S_3 (114) planes, respectively. These results collectively demonstrate the distinctive structure of the NiCrS/CN catalyst, featuring an ultrathin C-N overlayer coating over the NiCrS heterostructure surface.

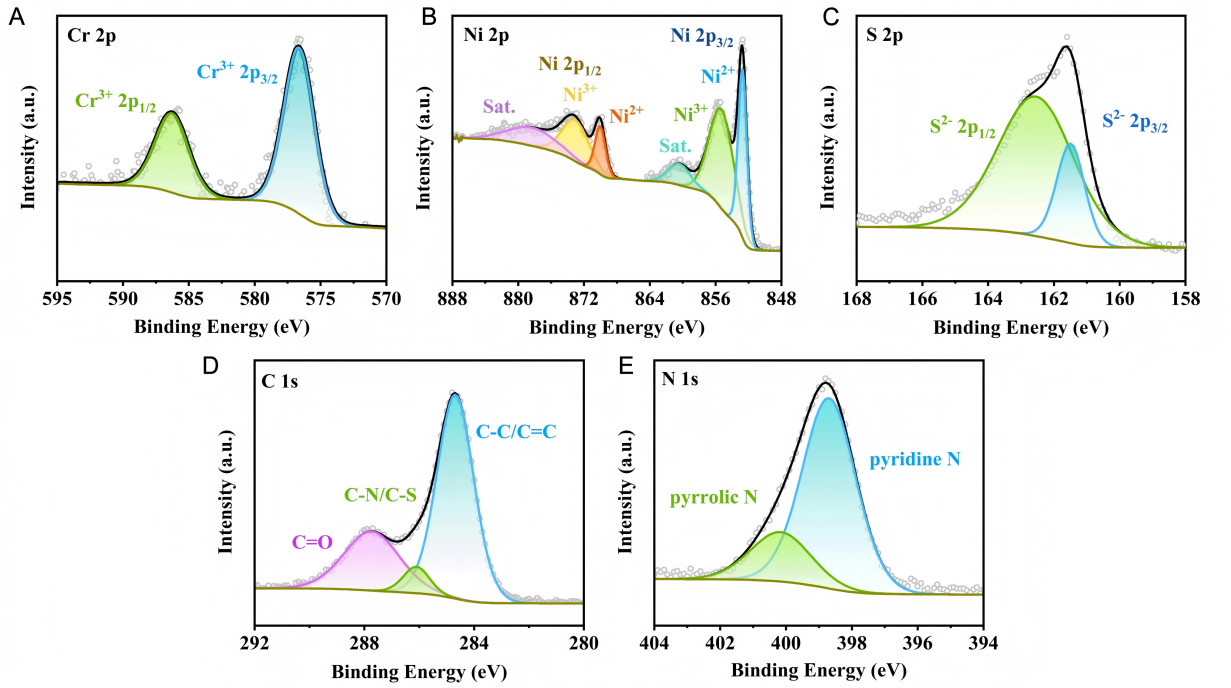

Figure 3. High-resolution XPS spectra of NiCrS/CN (A) Cr 2p spectrum; (B) Ni 2p spectrum; (C) S 2p spectrum; (D) C 1s spectrum; (E) N 1s spectrum. XPS: X-ray photoelectron spectroscopy; NiCrS/CN: nickel-chromium sulfide with nitrogen-doped carbon shell.

To explore the valence states and chemical compositions, X-ray photoelectron spectroscopy (XPS) analysis of NiCrS/CN was performed. The characteristic peaks at 576.7 and 586.5 eV in the high-resolution Cr 2p spectrum are indexed to the Cr-S bond, as depicted in Figure 3A. In the Ni 2p XPS spectrum [Figure 3B], well-resolved Ni^{2+} and Ni^{3+} species are observed with Ni 2p3/2 peaks at 852.8 and 855.6 eV, suggesting a typical NiS_2 phase. The S 2p XPS spectrum is fitted into two characteristic peaks [Figure 3C]. The characteristic peaks observed at 161.5 and 162.6 eV are assigned to the metal-sulfur bond in NiCrS [Figure 3C]. The C 1s spectrum of Figure 3D displays three components at 284.7, 286.1, and 287.8 eV, ascribed to C-C/C=C bond, C-N/C-S bond, and C=O bond. Moreover, N 1s signals in Figure 3E confirm the existence of pyridine N and pyrrolic N species.

The electrocatalytic performance of the obtained NiCrS/CN electrocatalyst for hydrogen evolution reaction (HER) was explored in a 1.0 M KOH electrolyte. To optimize catalytic activity, the influence of synthesis conditions (thiourea amount, calcination temperature, and calcination time) was systematically investigated. The effect of sulfidation/carbon coating conditions on determining HER activity was first explored in Supplementary Figures 1-3. Among all of the samples, the NiCrS/CN catalyst calcined at 350 °C for 2 h depicted the best HER performance in 1.0 M KOH electrolyte, and the optimal thiourea amount is 0.625 g. Unless otherwise stated, all subsequent electrochemical measurements were carried out under optimized conditions.

As illustrated in Figure 4A and B, the obtained NiCrS/CN catalyst with a takeoff potential of near 0 V can exceptionally derive a HER current density of -10 mA cm^{-2} at an overpotential of only 62 mV, 45 mV lower than that observed for NiCrS (107 mV). Notably, at overpotentials of 92 and 106 mV, NiCrS/CN achieves high HER current densities of -25 and -50 mA cm^{-2}, respectively, which are 3.91 and 4.85 times relative to those of NiCrS (-6.4 and -10.3 mA cm^{-2}). Strikingly, our NiCrS/CN electrocatalysts even demonstrate Pt-like HER kinetics at a high potential input [Supplementary Figure 4]. The corresponding HER current density at an overpotential of 188 mV could achieve as high as -200 mA/cm^2 for NiCrS/CN, which is even superior

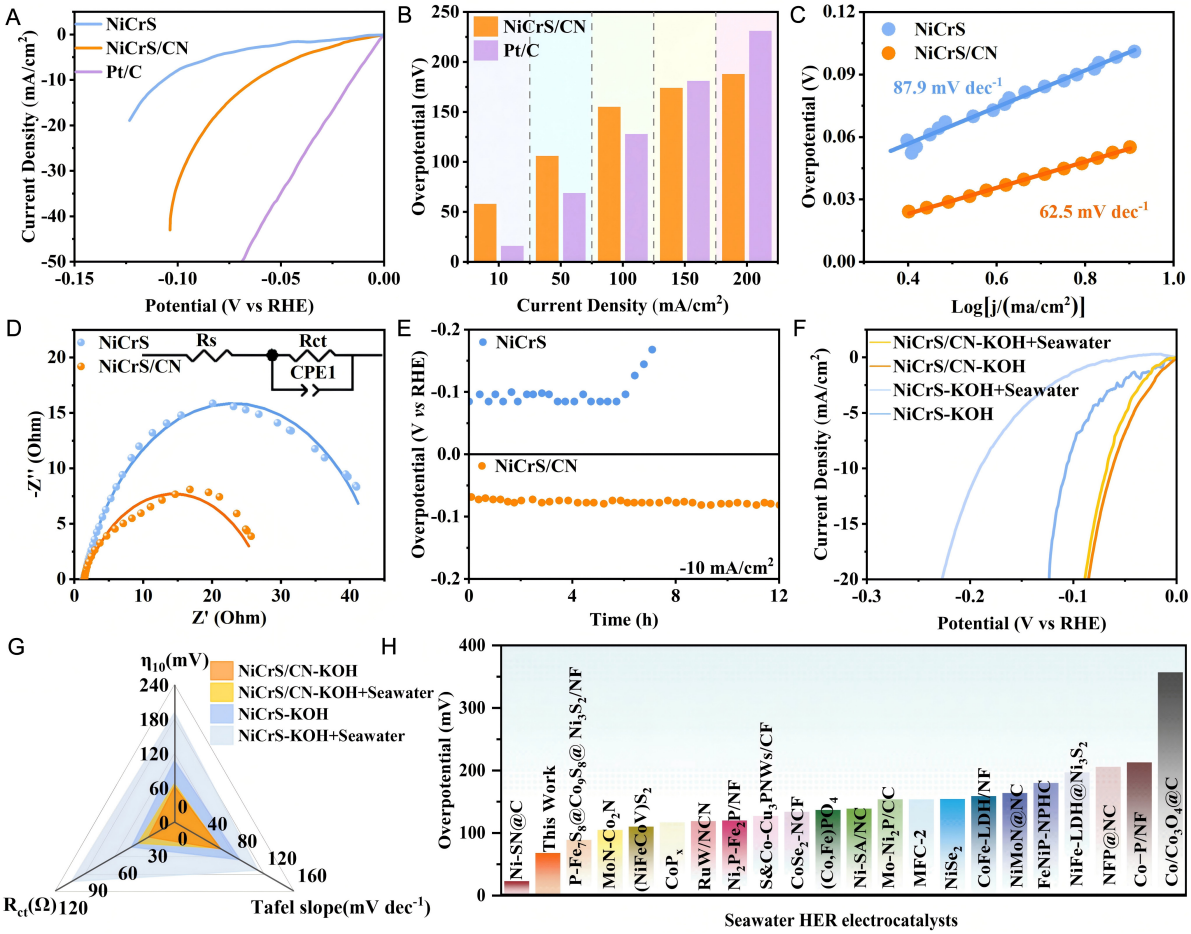

Figure 4. (A) HER LSV curves of Pt/C, NiCrS and NiCrS/CN under alkaline condition (1.0 M KOH) in three electrode configuration; (B) Comparison of overpotential of Pt/C and NiCrS/CN under different current densities; (C) Tafel plots of NiCrS and NiCrS/CN under alkaline condition (1.0 M KOH); (D) Nyquist diagram of NiCrS and NiCrS/CN under alkaline condition (1.0 M KOH); (E) Chronopotential results of NiCrS and NiCrS/CN under alkaline condition (1.0 M KOH) in three electrode configuration; (F) LSV curves of NiCrS/CN and NiCrS for HER in 1 M KOH and 1 M KOH + Seawater in three electrode configuration; (G) Comprehensive description of NiCrS/CN and NiCrS for HER in 1 M KOH and 1 M KOH + Seawater; (H) Comparison of NiCrS/CN with other transition metal-based catalysts in 1 M KOH + Seawater. HER: Hydrogen evolution reaction; RHE: reversible hydrogen electrode; LSV: linear sweep voltammetry.

relative to that for the benchmark Pt/C (-156.1 mA/cm^2). Tafel plots derived from linear sweep voltammetrys (LSVs) in Figure 4C showed a lower Tafel slope of 62.5 mV dec^{-1} for NiCrS/CN compared to NiCrS (87.9 mV dec^{-1}), suggesting that the C-N layer could efficiently facilitate Volmer-Heyrovsky progress over NiCrS-based electrocatalysts. To further explore the charge-transfer dynamics, electrochemical impedance spectra (EIS) were characterized [Figure 4D]. NiCrS/CN displays lower charge transfer resistance (R_{ct}) of 26.14 Ω compared to NiCrS (43.36 Ω), indicating rapid charge transfer kinetics between the catalyst and electrolyte via C-N layer coordination. Electrochemical activation surface area (ECSA) displayed a linear correlation with the double-layer capacitance (C_{dl}). As shown in Supplementary Figures 5-7, NiCrS/CN demonstrates a higher C_{dl} value of 44.48 mF cm^{-2} relative to that of NiCrS (33.32 mF cm^{-2}), revealing the exposure of more catalytic sites. Operational stability is critical to evaluate the practical application of catalysts. Long-term chronopotentiometry demonstrates that NiCrS/CN possesses robust stability, with only a 9.7% increase in overpotential during 12 h of electrocatalysis [Figure 4E]. In contrast, NiCrS even loses activity within 6 h, indicating the C-N layer may mitigate oxidation-driven degradation by shielding Ni/Cr metallic sites from direct exposure in an alkaline electrolyte, resulting in stable electrolysis of TMS-based electrocatalysts.

Compared to conventional freshwater electrolysis, alkaline seawater splitting could eliminate the intricacy of pretreatment, reduce system complexity, and reduce the operational cost of the electrolyzer for the industrialization of the "green hydrogen economy". Therefore, we systematically compared HER properties of NiCrS/CN and NiCrS under alkaline seawater conditions. As revealed in Figure 4F, the as-synthesized NiCrS/CN demonstrates extraordinary HER kinetics with an overpotential input of 68 mV at -10 mA cm^{-2} in alkaline seawater electrolyte. Strikingly, our NiCrS/CN electrocatalytic system only require an ultralow overpotential input of 143, 164 and 191 mV to afford industrial-relevant current density of -50, -100, and -200 mA cm^{-2}, which is 12.20, 15.87 and 19.8 times relative to those of NiCrS (-4.1, -6.3 and -10.1 mA/cm^2), respectively, at the same overpotential input, due to a fast electron transfer ability as well as enhanced HER kinetic [Supplementary Figures 8-11]. More interestingly, it is noteworthy that NiCrS/CN shows similar HER behaviors in freshwater and seawater, and only a diminished degradation trend (~ 7 mV) in alkaline seawater is observed versus that in 1.0 M KOH electrolyte. Conversely, NiCrS demonstrates lower HER kinetics in alkaline seawater compared with alkaline freshwater [Figure 4G, Supplementary Figures 12 and 13]. To afford current densities of -10 and -50 mA cm^{-2}, larger overpotentials of 196 and 279 mV are needed in alkaline seawater solution relative to freshwater over the NiCrS system. Such a difference is attributed to C-N, as a protective layer, could compel the blocking species (e.g., bacteria, Cl^-, Mg^{2+} and Ca^{2+} ions in seawater) from surface active sites and achieve a fast HER progress in alkaline seawater media. Overall, by virtue of C-N layer, our NiCrS-based electrocatalytic system demonstrate remarkable catalytic performance in alkaline freshwater and seawater electrolyte, which can compare with other state-of-the-art electrocatalysts such as Ni-SN@C[35], P-Fe_7S_8@Co_9S_8@Ni_3S_2/NF[36], RuW/NCN[37], Ni-SA/NC[38], MFC-2[39], NFP@NC[40], Mo-based elctrocatalysts[41-43], NiFe-based elctrocatalysts[44-47], Se-based elctrocatalysts[48,49], Co-based elctrocatalysts[50-52], and Co-P-based[53-55] elctrocatalysts [Figure 4H and Supplementary Table 1].

OER has been identified as a major bottleneck in electrolyzers due to its intrinsic multiple proton-coupled electron transfer process. The sluggish kinetics will require a large theoretical energy barrier associated with a lower hydrogen production efficiency of an electrolyzer. Therefore, we further evaluate the OER performance over NiCrS/CN electrocatalytic systems in a 1.0 M KOH electrolyte [Supplementary Figures 14-16]. As depicted in Supplementary Figures 17-20, the incorporation of a C-N layer can effectively promote OER kinetics of the NiCrS-based electrocatalytic system with an overpotential of 106 mV for 10 mA cm^{-2} combined with robust stability in alkaline solution, making it as a promising candidate for water oxidation [Supplementary Table 2]. The polarization results and performance in Figure 5A and Supplementary Figures 21-24 further confirm that minimal degradation is observed in alkaline seawater media over the NiCrS/CN electrocatalytic system rather than NiCrS. Obviously, industrial-scale current densities of 50 and 100 mA cm^{-2} could be afforded over the NiCrS/CN electrode at low overpotentials of 162 and 225 mV, respectively, in alkaline seawater solution. Exceptionally, the overpotential of NiCrS/CN in alkaline seawater at as high as 200 mA cm^{-2} is still lower than the maximum theoretically overpotential of 480 mV required for initial hypochlorite production, suggesting the NiCrS/CN electrode as a solid barrier to Cl^- corrosion.

Given the excellent HER/OER activities of NiCrS/CN, we explored the overall water splitting performance in alkaline freshwater and seawater electrolyte through a two-electrode configuration, where NiCrS/CN is used as both the cathode and anode. Remarkably, the assembled NiCrS/CN electrolyzer demonstrates outstanding overall water splitting activities in alkaline freshwater and seawater electrolyte. Notably, our NiCrS/CN electrolyzer can produce an industrial current density of 100 mA/cm^2, with a 50 mV lower energy potential than the NiCrS electrolyzer in alkaline freshwater [Figure 5B]. Even under seawater condition, a highly efficient NiCrS/CN electrolyzer only requires cell voltages of 1.40, 1.49 and 1.55 V to produce current densities of 50, 100 and 150 mA/cm^2, 2.53, 2.59 and 2.48 times superior to those of NiCrS electrolyzer (19.8, 38.5 and 60.4 mA/cm^2) at the same potential input [Figure 5C]. As shown in Figure 5D and

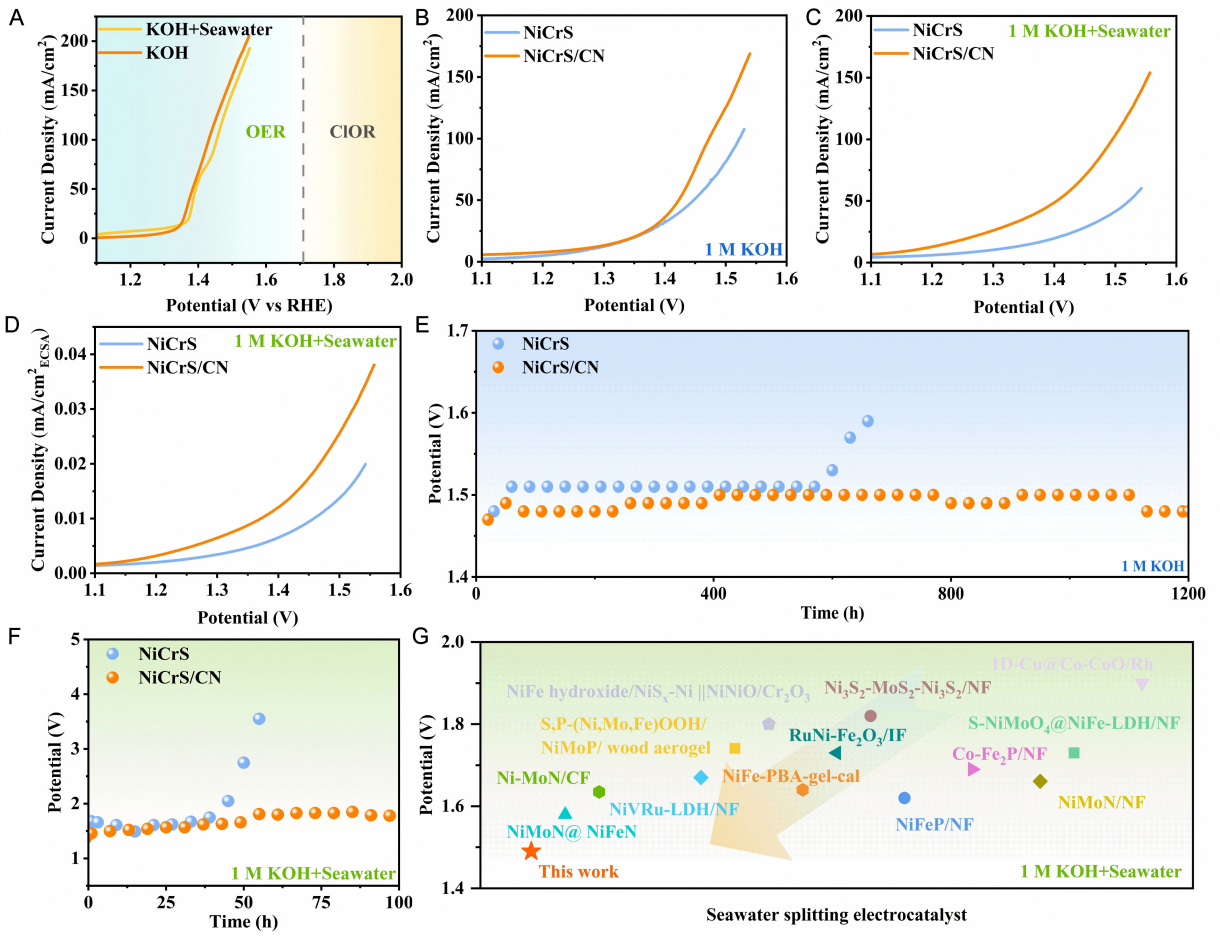

Figure 5. (A) OER LSV curves of NiCrS/CN in 1 M KOH and 1 M KOH + Seawater in three electrode configuration; (B and C) LSV curves of NiCrS and NiCrS/CN for overall water splitting in 1 M KOH and 1 M KOH + Seawater in two electrode configuration; (D) ECSA normalized LSV curves of NiCrS and NiCrS/CN for overall water splitting in 1 M KOH + Seawater in two electrode configuration; (E and F) Chronopotential curves of NiCrS and NiCrS/CN at 50 mA cm^{-2} in 1 M KOH and 1 M KOH + Seawater in two electrode configuration; (G) Comparison of the potential to attain 100 mA cm^{-2} current density of overall water splitting between NiCrS/CN and other catalysts. OER: Oxygen evolution reaction; ECSA: electrochemical activation surface area; RHE: reversible hydrogen electrode; LSV: linear sweep voltammetry.

Supplementary Figure 25, NiCrS/CN still showed higher ECSA-normalized current densities than NiCrS in both alkaline freshwater and alkaline seawater for overall water splitting. For example, at a potential input of 1.55 V, NiCrS/CN can produce a normalized current density of 0.038 mA/cm^2_{ECSA} in 1 M KOH + seawater, which is 2 times higher than that of NiCrS (0.019 mA/cm^2_{ECSA}). A similar trend is also observed in alkaline freshwater [Supplementary Figure 25]. Supplementary Figure 26 shows a representative GC result over NiCrS/CN for water splitting in alkaline solution. After 1 h of chronoamperometric electrolysis, only hydrogen (H_2) and oxygen (O_2) peaks were detected in the released gas without other impurity gases present, further confirming the high efficiency of NiCrS/CN in electrocatalyzing water splitting into hydrogen production. Furthermore, the assembled NiCrS/CN electrolyzer displays alkali-tolerant ability under extreme conditions (3 M KOH + seawater), indicating a promising application in industrial [Supplementary Figure 27]. Strikingly, the assembled NiCrS/CN configuration demonstrates an outstanding robustness toward electrocatalytic overall water splitting in both freshwater and seawater electrolytes. As revealed in Figure 5E, our NiCrS/CN system can stably maintain a superior 1,200 h electrolysis (50 mA cm^{-2}@V) without obvious degradation compared to that of the NiCrS electrolyzer in alkaline freshwater solutions. Even when conducted under alkaline seawater conditions, the assembled NiCrS/CN electrolyzer can be stably operated for at least 100 h to achieve industrially relevant hydrogen production from seawater splitting [Figure 5F]. In

contrast, the NiCrS system loses its activity after only 39 h of electrocatalysis in harsh conditions. Such robust stability of NiCrS/CN is attributed to the encapsulation of C-N overlayers, which could efficiently anchor S species via strong C-S bonds at the interface. Such a unique configuration benefits in suppressing S species dissolution and leaching into alkaline electrolytes, guaranteeing superior durability. Overall, NiCrS/CN exhibits high-performing electrocatalytic seawater splitting kinetics, which are superior to some Ru-based[56,57], Co-based[58,59], NiFe-based[60,61,62], NiMoN-based[63-65], and other alkaline water splitting systems[66,67,68] reported [Figure 5G].

In this work, our NiCrS/CN system demonstrates a striking catalytic performance toward water splitting in both alkaline freshwater and seawater electrolytes. This remarkable enhancement in catalytic kinetics arises from the following features: On the one hand, the C-N layer can induce a strong synergistic effect between metallic active sites and the C-N overlayer. In detail, C-N overlayers could accelerate electron transfer kinetics and withdraw charge to NiCr active sites, which reconfigures a unique charge distribution of metallic active sites with highly efficient spatial electron separation. Therefore, C-N species could configure the orbital distributions (d-band center) of NiCr sites with higher electron states and supply more coordinatively unsaturated sites. Such a unique local electronic configuration could generate a more negative position of the valence band edge near the Fermi level, which endows stronger electron-donating capability of NiCr active sites associated with a lower energy barrier for H_2O molecular dissociation, and thereby optimizes adsorption/desorption capability of intermediated *OH and *H species. Subsequently, the in situ generated H intermediate species could migrate through spillover pathways and desorb from the C-N overlayer to form gaseous H_2, achieving a favorable hydrogen spillover dynamic progress. On the other hand, C-N species could efficiently improve the hydrophilicity of NiCr-based electrocatalysts and enhance the adsorption ability of H_2O molecules on NiCr sites. Also, it is well known that accumulated hydrogen bubbles on the electrode surface could hamper the interaction between the electrolyte and electrode surface, even blocking the catalytic active sites. Therefore, the introduction of C-N overlayers could endow fast kinetics of H_2 molecular release from the catalytic surface, resulting in a robust performance toward electrolyzing hydrogen evolution. More importantly, it is found that the C-N layer can serve as a Lewis base layer to manipulate the alkaline local micro-environment of the NiCr-based electrocatalytic system. Especially, pyridine N species in the C-N layer possess abundant lone-pair electrons that benefit the coordinated dynamics of chlorine on the metallic surface. Such a novel "electron-rich" local configuration could effectively repel Cl^- ions and provide a specific protective layer against Cl^- adsorption. Furthermore, the C-N overlayer could simultaneously stimulate S atom migration via the formation of C-S bonds. The strong C-S interaction could benefit the inhibition of sulfur species leaching into alkaline electrolyte, therefore, achieving a robust electrocatalytic seawater splitting for hydrogen generation in industry.

CONCLUSION

In summary, we successfully engineered a C-N overlayer encapsulated on NiCrS to endow a high-performance seawater splitting. Thanks to the synergistic effect between the encapsulated C-N overlayers and NiCrS, an optimized local electronic micro-environment has been achieved. Such a unique local electronic configuration could enhance the electron-donating affinity of NiCr active sites and facilitate the reactive kinetics of H_2O adsorption/dissociation, thereby resulting in a thermodynamic balance of intermediate *OH and *H species. More importantly, C-N overlayers are utilized to regulate the chemical state of surficial sites for adsorbed Cl- species, efficiently suppressing Cl corrosion. Meanwhile, the C-N overlayer could simultaneously stimulate S atom migration via the formation of C-S bonds, preventing sulfur species leaching. As a result, the obtained NiCrS/CN electrocatalysts show a striking seawater splitting performance. In 1.0 M KOH electrolyte, the NiCrS/CN catalyst exhibits remarkable HER activity. At a high overpotential input (≥ 180 mV), Pt-like HER kinetics are observed on NiCrS/CN electrocatalysts. Furthermore, the assembled NiCrS/CN cell achieves industrially relevant current densities of 50, 100, and

150 mA/cm^2 at cell voltages of 1.40, 1.49, and 1.55 V, respectively, demonstrating excellent stability and durability. Notably, the assembled NiCrS/CN electrolyzer demonstrates a robust industrially relevant operational performance and could be operated for at least 1,200 h and 100 h in alkaline freshwater and seawater electrolytes, respectively. This work represents a novel design strategy for developing highly active and robust cost-effective catalysts for large-scale seawater electrolysis.

DECLARATIONS

Authors' contributions

Original draft, investigation, data curation, formal analysis, methodology and conceptualization: Cheng, S.
Original draft, conceptualization, review and editing: Tang, S.
Formal analysis and data curation: Ding, X.
Conceptualization and supervision: Jiang, N.
Data curation and visualization: Qin, H.
Editing, and supervision: Yin, Y.
Review, supervision, formal analysis, conceptualization: Song, F.

Availability of data and materials

The raw data supporting the findings of this study are available within this Article and its Supplementary Materials. Further data are available from the corresponding authors upon request.

AI and AI-assisted tools statement

Not applicable.

Financial support and sponsorship

The work described in this paper was supported by the National Natural Science Foundation of China (No. 52362028 and 22201294)

Conflicts of interest

All authors declared that there are no conflicts of interest.

Ethical approval and consent to participate

Not applicable.

Consent for publication

Not applicable.

Supplementary Materials

Supplementary Materials

REFERENCES

1. Tian, H.; Li, W.; Lee, Y.; et al. Conformally coated scaffold design using water-tolerant $Pr_{1.8}Ba_{0.2}NiO_{4.1}$ for protonic ceramic electrochemical cells with 5,000-h electrolysis stability. *Nat. Energy.* **2025**, *10*, 890-903. DOI
2. Dong, J.; Ding, X.; Liu, L.; et al. Engineering the electronic regulation of ultrafine Ru nanoparticles for boosting hydrogen oxidation and evolution electrocatalysis. *Chem. Commun.* **2026**, *62*, 7106-10. DOI
3. Long, J.; Wu, H.; Liu, Y.; et al. Hydrogen production from chemical hydrogen storage materials over copper-based catalysts. *cMat* **2024**, *1*, e10. DOI
4. Qin, H.; Tang, S.; Xu, L.; et al. Alkaline titanium carbide (MXene) engineering ultrafine non-noble nanocatalysts toward remarkably boosting hydrogen evolution from ammonia borane hydrolysis. *J. Alloys. Compd.* **2025**, *1010*, 177644. DOI
5. Chai, H.; Hu, J.; Zhang, R.; et al. Efficient hydrogen production from formic acid dehydrogenation over ultrasmall PdIr nanoparticles on amine-functionalized yolk-shell mesoporous silica. *J. Colloid. Interface. Sci.* **2025**, *678*, 261-71. DOI

6. Quan, L.; Jiang, H.; Mei, G.; Sun, Y.; You, B. Bifunctional electrocatalysts for overall and hybrid water splitting. *Chem. Rev.* **2024**, *124*, 3694-812. DOI
7. Tang, S.; Zhang, Z.; Lv, Q.; et al. Heteroatom engineering in earth-abundant cobalt electrocatalyst for energy-saving hydrogen evolution coupling with urea oxidation. *ACS. Appl. Mater. Interfaces.* **2024**, *16*, 66008-17. DOI
8. Yao, Q.; Zhu, F.; Long, J.; Huo, J.; Huang, M.; Lu, Z. Efficient ammonia borane dehydrogenation on Ni/P-Mo@Mo_2C: the effect of P dopant and Mo@Mo_2C heterostructure. *Chem. Eng. J.* **2025**, *520*, 166442. DOI
9. Guan, S.; Liu, Y.; Liu, S.; et al. MXene-supported Ru-Ni: a common active site for hydrolysis, hydrogen oxidation, and hydrogenation. *Angew. Chem. Int. Ed.* **2025**, *64*, e202506869. DOI
10. Li, X.; Liu, Z.; Shao, S.; et al. A Ca-modified Ni/CeO_2·Al_2O_3 bifunctional catalyst for two-stage steam reforming of biomass pyrolysis oil for hydrogen production. *Ind. Crops. Prod.* **2025**, *228*, 120891. DOI
11. Xiao, C.; Guo, X.; Tang, X.; et al. Fabrication of $Mo_{0.1}$-$Cu_{0.4}Ni_{0.6}Co_2O_4$ catalyst based on dual-doping engineering for fast hydrogen release from ammonia borane methanolysis. *Mater. Today. Chem.* **2026**, *52*, 103443. DOI
12. Niu, Q.; Gao, F.; Sun, X.; Zheng, Y.; Qiao, S. Chloride-mediated electron buffering on Ni-Fe anodes for ampere-level alkaline seawater electrolysis. *Adv. Funct. Mater.* **2025**, *35*, 2504872. DOI
13. Fu, J.; Kong, X.; Liu, X.; et al. Design of oxides/hydroxides-based seawater oxidation electrocatalysts: from mechanism understanding, selectivity to activity. *Adv. Funct. Mater.* **2026**, *36*, e23937. DOI
14. Li, M.; Liu, C.; Teng, Z.; et al. Manipulating interfacial water configuration via constructing asymmetric structure unit for hydrogen production in alkaline seawater. *Adv. Funct. Mater.* **2025**, *35*, e14517. DOI
15. Xu, J.; Kao, C. C.; Shen, H.; Liu, H.; Zheng, Y.; Qiao, S. Z. $Ru_{0.1}Mn_{0.9}O_x$ electrocatalyst for durable oxygen evolution in acid seawater. *Angew. Chem. Int. Ed.* **2025**, *64*, e202420615. DOI
16. Liu, X.; Chi, J.; Mao, H.; Wang, L. Principles of designing electrocatalyst to boost reactivity for seawater splitting. *Adv. Energy. Mater.* **2023**, *13*, 2301438. DOI
17. Liu, W.; Yu, J.; Li, T.; et al. Self-protecting CoFeAl-layered double hydroxides enable stable and efficient brine oxidation at 2 A cm^{-2}. *Nat. Commun.* **2024**, *15*, 4712. DOI
18. Li, X.; Wu, T.; Li, N.; et al. Vertically staggered porous Ni_2P/Fe_2P nanosheets with trace Ru doping as bifunctional electrocatalyst for alkaline seawater splitting. *Adv. Funct. Mater.* **2024**, *34*, 2400734. DOI
19. Sun, X.; Shen, W.; Liu, H.; et al. Corrosion-resistant NiFe anode towards kilowatt-scale alkaline seawater electrolysis. *Nat. Commun.* **2024**, *15*, 10351. DOI PubMed PMC
20. Huang, L.; Bao, D.; Jiang, Y.; Regenauer-Lieb, K.; Zheng, Y.; Qiao, S. Z. The utilization of ions in seawater for electrocatalysis. *Natl. Sci. Rev.* **2025**, *12*, nwaf461. DOI PubMed PMC
21. Dionigi, F.; Reier, T.; Pawolek, Z.; Gliech, M.; Strasser, P. Design criteria, operating conditions, and nickel-iron hydroxide catalyst materials for selective seawater electrolysis. *ChemSusChem* **2016**, *9*, 962-72. DOI PubMed
22. Liu, H.; Shen, W.; Jin, H.; et al. High-performance alkaline seawater electrolysis with anomalous chloride promoted oxygen evolution reaction. *Angew. Chem. Int. Ed.* **2023**, *62*, e202311674. DOI
23. Jin, H.; Xu, J.; Liu, H.; et al. Emerging materials and technologies for electrocatalytic seawater splitting. *Sci. Adv.* **2023**, *9*, eadi7755. DOI PubMed PMC
24. Wu, Q.; Zhong, Y.; Chen, R.; et al. Cu-Ag-C@Ni_3S_4 with core shell structure and rose derived carbon electrode materials: an environmentally friendly supercapacitor with high energy and power density. *Ind. Crops. Prod.* **2024**, *222*, 119676. DOI
25. Xie, N.; Ma, D.; Wu, Y.; Wu, X.; Zhu, Q. Hierarchical Cu_2S hollow nanowire arrays for highly efficient hydrogen evolution reaction. *Sustain. Energy. Fuels.* **2021**, *5*, 2633-9. DOI
26. Yuan, X.; Zhou, S.; Wang, S.; et al. Ordered macroporous superstructure of defective carbon adorned with tiny cobalt sulfide for selective electrocatalytic hydrogenation of cinnamaldehyde. *Appl. Catal. B. Environ.* **2025**, *361*, 124642. DOI
27. Wang, S.; Geng, Z.; Bi, S.; et al. Recent advances and future prospects on Ni_3S_2-Based electrocatalysts for efficient alkaline water electrolysis. *Green. Energy. Environ.* **2024**, *9*, 659-83. DOI
28. Cao, C.; Xu, Q.; Zhu, Q. Ultrathin two-dimensional metallenes for heterogeneous catalysis. *Chem. Catalysis.* **2022**, *2*, 693-723. DOI
29. Xie, N.; Ma, D. D.; Wu, X. T.; Zhu, Q. L. Facile construction of self-supported Fe-doped Ni_3S_2 nanoparticle arrays for the ultralow-overpotential oxygen evolution reaction. *Nanoscale* **2021**, *13*, 1807-12. DOI PubMed
30. Guan, D.; Ryu, G.; Hu, Z.; et al. Utilizing ion leaching effects for achieving high oxygen-evolving performance on hybrid nanocomposite with self-optimized behaviors. *Nat. Commun.* **2020**, *11*, 3376. DOI PubMed PMC
31. Li, Y.; Zhou, H.; Cai, S.; et al. Electrolyte-assisted polarization leading to enhanced charge separation and solar-to-hydrogen conversion efficiency of seawater splitting. *Nat. Catal.* **2024**, *7*, 77-88. DOI

32. Xu, S. W.; Li, J.; Zhang, N.; Shen, W.; Zheng, Y.; Xi, P. Recent advances in direct seawater splitting for producing hydrogen. *Chem. Commun.* **2023**, *59*, 9792-802. DOI
33. Guo, Y.; Park, T.; Yi, J. W.; et al. Nanoarchitectonics for transition-metal-sulfide-based electrocatalysts for water splitting. *Adv. Mater.* **2019**, *31*, e1807134. DOI
34. Shen, W.; Wang, C.; Xu, Q.; Liu, H.; Wang, Y. Nitrogen-doping-induced defects of a carbon coating layer facilitate na-storage in electrode materials. *Adv. Energy. Mater.* **2015**, *5*, 1400982. DOI
35. Jin, H.; Wang, X.; Tang, C.; et al. Stable and highly efficient hydrogen evolution from seawater enabled by an unsaturated nickel surface nitride. *Adv. Mater.* **2021**, *33*, e2007508. DOI
36. Wu, Y.; Du, X.; Zhang, X. P doping transition metal sulfides as bifunctional electrocatalyst for overall seawater splitting. *Int. J. Hydrogen. Energy.* **2025**, *103*, 174-82. DOI
37. Wang, H.; Yang, P.; Liu, D.; et al. Ultrasmall RuM (Mo, W, Cr) decorated on nitrogen-doped carbon nanosheet with strong metal-support interactions for electrocatalytic hydrogen generation in wide pH range. *J. Colloid. Interface. Sci.* **2023**, *651*, 686-95. DOI
38. Zang, W.; Sun, T.; Yang, T.; et al. Efficient hydrogen evolution of oxidized Ni-N_3 defective sites for alkaline freshwater and seawater electrolysis. *Adv. Mater.* **2021**, *33*, e2003846. DOI
39. Pal, S.; Shimizu, K.; Khatun, S.; Singha, S.; Watanabe, S.; Roy, P. Electrolyte engineering for effective seawater splitting based on manganese iron chromium layered triple hydroxides as novel bifunctional electrocatalysts. *J. Mater. Chem. A.* **2023**, *11*, 12151-63. DOI
40. Zhang, H.; Wang, Y.; Zhang, B.; et al. Interwoven N-doped carbon nanotubes with capped Ni-doped FeP as double-functional electrocatalysts for overall seawater electrolysis. *Sci. China. Mater.* **2023**, *66*, 4630-8. DOI
41. Wang, X.; Han, X.; Du, R.; et al. Cobalt molybdenum nitride-based nanosheets for seawater splitting. *ACS. Appl. Mater. Interfaces.* **2022**, *14*, 41924-33. DOI
42. Li, X.; Wu, Y.; Li, S.; et al. Efficient hydrogen evolution of Ni_2P *via* incorporation of Mo for alkaline freshwater and seawater electrolysis. *New. J. Chem.* **2022**, *46*, 20602-9. DOI
43. Jiang, B.; Cui, Y.; Shi, S.; Jiang, N.; Tan, W. Preparation of highly active transition bimetallic nitride NiMoN hydrogen evolution reaction (HER) catalyst and its performance study in seawater electrolysis. *Acta. Chim. Sinica.* **2022**, *80*, 1394. DOI
44. Feng, C.; Chen, M.; Zhou, Y.; et al. High-entropy NiFeCoV disulfides for enhanced alkaline water/seawater electrolysis. *J. Colloid. Interface. Sci.* **2023**, *645*, 724-34. DOI
45. Wu, L.; Yu, L.; Zhang, F.; et al. Heterogeneous bimetallic phosphide Ni_2P-Fe_2P as an efficient bifunctional catalyst for water/seawater splitting. *Adv. Funct. Mater.* **2021**, *31*, 2006484. DOI
46. Yu, Q.; Liu, X.; Liu, G.; et al. Constructing three-phase heterojunction with 1D/3D hierarchical structure as efficient trifunctional electrocatalyst in alkaline seawater. *Adv. Funct. Mater.* **2022**, *32*, 2205767. DOI
47. Ren, L.; Wang, C.; Li, W.; et al. Heterostructural NiFe-LDH@Ni_3S_2 nanosheet arrays as an efficient electrocatalyst for overall water splitting. *Electrochim. Acta.* **2019**, *318*, 42-50. DOI
48. Chen, H.; Zhang, S.; Liu, Q.; et al. $CoSe_2$ nanocrystals embedded into carbon framework as efficient bifunctional catalyst for alkaline seawater splitting. *Inorg. Chem. Commun.* **2022**, *146*, 110170. DOI
49. Zhang, S.; Li, R.; Li, X.; et al. Hydrothermally synthesized $NiSe_2$ nanospheres for efficient bifunctional electrocatalysis in alkaline seawater electrolysis: high performance and stability in HER and OER. *Mater. Res. Bull.* **2025**, *189*, 113463. DOI
50. Wang, N.; He, X.; Chen, Y.; et al. S and Co co-doped Cu_3P nanowires self-supported on Cu foam as an efficient hydrogen evolution electrocatalyst in artificial seawater. *J. Porous. Mater.* **2021**, *28*, 763-71. DOI
51. Liu, W.; Jiang, K.; Hu, Y.; et al. Zr-doped CoFe-layered double hydroxides for highly efficient seawater electrolysis. *J. Colloid. Interface. Sci.* **2021**, *604*, 767-75. DOI
52. Zhang, Q.; Zhao, X.; Miao, X.; Yang, W.; Wang, C.; Pan, Q. ZIF-L-Co@carbon fiber paper composite derived Co/Co_3O_4@C electrocatalyst for ORR in alkali/acidic media and overall seawater splitting. *Int. J. Hydrogen. Energy.* **2020**, *45*, 33028-36. DOI
53. Wu, L.; Yu, L.; Mcelhenny, B.; et al. Rational design of core-shell-structured CoP @FeOOH for efficient seawater electrolysis. *Appl. Catal. B. Environ.* **2021**, *294*, 120256. DOI
54. Kim, C.; Lee, S.; Kim, S. H.; et al. Cobalt-iron-phosphate hydrogen evolution reaction electrocatalyst for solar-driven alkaline seawater electrolyzer. *Nanomaterials* **2021**, *11*, 2989. DOI
55. Liang, Y.; Zhang, L.; Liu, Q.; et al. Amorphous Co-P film: an efficient electrocatalyst for hydrogen evolution reaction in alkaline seawater. *Eur. J. Inorg. Chem.* **2023**, *26*, e202200657. DOI
56. Wang, D.; Li, Q.; Han, C.; Lu, Q.; Xing, Z.; Yang, X. Atomic and electronic modulation of self-supported nickel-vanadium layered double hydroxide to accelerate water splitting kinetics. *Nat. Commun.* **2019**, *10*, 3899. DOI PubMed PMC
57. Cui, T.; Zhai, X.; Guo, L.; et al. Controllable synthesis of a self-assembled ultralow Ru, Ni-doped Fe_2O_3 lily as a bifunctional electrocatalyst for large-current-density alkaline seawater electrolysis. *Chin. J. Catal.* **2022**, *43*, 2202-11. DOI

58. Wang, S.; Yang, P.; Sun, X.; et al. Synthesis of 3D heterostructure Co-doped Fe_2P electrocatalyst for overall seawater electrolysis. *Appl. Catal. B. Environ.* **2021**, *297*, 120386. DOI
59. Tran, P. K. L.; Tran, D. T.; Malhotra, D.; et al. Highly effective freshwater and seawater electrolysis enabled by atomic Rh-modulated Co-CoO lateral heterostructures. *Small* **2021**, *17*, e2103826. DOI
60. Kuang, Y.; Kenney, M. J.; Meng, Y.; et al. Solar-driven, highly sustained splitting of seawater into hydrogen and oxygen fuels. *Proc. Natl. Acad. Sci. U. S. A.* **2019**, *116*, 6624-9. DOI PubMed PMC
61. Zhang, H.; Geng, S.; Ouyang, M.; Yadegari, H.; Xie, F.; Riley, D. J. A self-reconstructed bifunctional electrocatalyst of pseudo-amorphous nickel carbide @ iron oxide network for seawater splitting. *Adv. Sci.* **2022**, *9*, e2200146. DOI
62. Liu, J.; Liu, X.; Shi, H.; et al. Breaking the scaling relations of oxygen evolution reaction on amorphous NiFeP nanostructures with enhanced activity for overall seawater splitting. *Appl. Catal. B. Environ.* **2022**, *302*, 120862. DOI
63. Yu, L.; Zhu, Q.; Song, S.; et al. Non-noble metal-nitride based electrocatalysts for high-performance alkaline seawater electrolysis. *Nat. Commun.* **2019**, *10*, 5106. DOI PubMed PMC
64. Wu, L.; Zhang, F.; Song, S.; et al. Efficient alkaline water/seawater hydrogen evolution by a nanorod-nanoparticle-structured Ni-MoN catalyst with fast water-dissociation kinetics. *Adv. Mater.* **2022**, *34*, e2201774. DOI
65. Yu, L.; Wu, L.; Mcelhenny, B.; et al. Ultrafast room-temperature synthesis of porous S-doped Ni/Fe (oxy)hydroxide electrodes for oxygen evolution catalysis in seawater splitting. *Energy. Environ. Sci.* **2020**, *13*, 3439-46. DOI
66. Chen, H.; Zou, Y.; Li, J.; et al. Wood aerogel-derived sandwich-like layered nanoelectrodes for alkaline overall seawater electrosplitting. *Appl. Catal. B. Environ.* **2021**, *293*, 120215. DOI
67. Li, Y.; Wu, X.; Wang, J.; et al. Sandwich structured Ni_3S_2-MoS_2-Ni_3S_2@Ni foam electrode as a stable bifunctional electrocatalyst for highly sustained overall seawater splitting. *Electrochimica. Acta.* **2021**, *390*, 138833. DOI
68. Wang, H.; Chen, L.; Tan, L.; et al. Electrodeposition of NiFe-layered double hydroxide layer on sulfur-modified nickel molybdate nanorods for highly efficient seawater splitting. *J. Colloid. Interface. Sci.* **2022**, *613*, 349-58. DOI